Hydrogen Sulfide Passivation for p-type Passivated Emitter and Rear Contact (PERC) Solar Cells

Tasnim K. Mouri[1,2], Ajay Upadhyaya[3], Ajeet Rohatgi[3], YoungWoo Ok[3], Amandee Hua[4], Dirk Hauschild[4,5,6], Lothar Weinhardt[4,5,6], Clemens Heske[4,5,6], Vijaykumar Upadhyaya[3], Brian Rounsaville[3], Ujjwal K. Das[1]

[1]Institute of Energy Conversion, University of Delaware, Newark, DE 19716, USA
[2]Materials Science & Engineering, University of Delaware, Newark, DE 19716, USA
[3]School of Electrical and Computer Engineering, Georgia Institute of Technology, Atlanta, GA 30332, USA
[4]Department of Chemistry and Biochemistry, University of Nevada Las Vegas (UNLV), Las Vegas, NV 89154-4003, USA
[5]Institute for Photon Science and Synchrotron Radiation (IPS), Karlsruhe Institute of Technology (KIT), 76344 Eggenstein-Leopoldshafen, Germany
[6]Institute for Chemical Technology and Polymer Chemistry (ITCP), Karlsruhe Institute of Technology (KIT), 76128 Karlsruhe, Germany

***Abstract*— *This work reports on the application of sulfur (S)-passivation to passivated emitter and rear contact (PERC) solar cells. The emitter surface was passivated by hydrogen sulfide (H_2S) gas phase reaction and capped by a hydrogenated amorphous silicon nitride (a-SiN_x:H) layer. The sulfur passivation on a symmetrically n^+ diffused emitter is shown to lead to a saturation current density (J_0) of 30 fA/cm^2 at $R_{sheet,n+} \approx 100$ Ω/sq. The application of S-passivation to the emitter surface in the PERC cell structure, with the rear surface passivated by an aluminum oxide (Al_2O_3)/a-SiN_x:H stack, showed a promising implied open-circuit voltage (V_{OC}) of ≈ 680 mV (highest: 686 mV), which was higher than that for the a-SiN_x:H or SiO_2/a-SiN_x:H passivated emitter surfaces. However, a significant drop in cell V_{OC} is observed for the S-passivated PERC cell after the completion of device fabrication with laser patterning, screen-printed metal contact deposition, and firing. Nonetheless, an efficiency of ~20% and a V_{OC} of ~650 mV was achieved with an emitter surface passivated by sulfur. We identified that the 760^{O}C contact firing process degrades the S-passivation quality. The surface morphology was studied and a detailed surface analysis were performed to study the details of the S-passivated surface degradation.*

***Index Terms*— *n^+ diffused emitter, hydrogen sulfide reaction passivation, screen printed metal contact firing, X-ray photoelectron spectroscopy, p-PERC cell.*

I. INTRODUCTION

After being introduced in the 1980s and further developed for ~25 years, passivated emitter and rear cell (PERC) solar cells have made their way into mass production [1]. The global production capacity for PERC cells has reached nearly 120 GW in 2022, which was possible by continuous improvements in cell and module efficiency [2]. The current record efficiency of 24.5% for p-type PERC (p-PERC) solar cells is held by China's Trina Solar [3]. One of the key factors for these record-breaking efficiencies is the passivation of the Si surface to reduce surface recombination rates by terminating surface defects and/or dangling bonds [4]. Improved surface passivation can be achieved by repelling one type of charge carriers away from the surface by a fixed charge in the passivating film (field-effect passivation) and/or by reducing the interface defect density (chemical passivation) [5].

Over time, many materials and passivation processes have been evaluated with the goal of achieving a high open-circuit voltage (V_{OC}). Several materials, such as hydrogenated amorphous silicon nitride (a-SiN_X:H), aluminum oxide (Al_2O_3), silicon dioxide (SiO_2), and hydrogenated amorphous silicon (a-Si:H), have been found to be promising candidates. Though each of these materials can effectively reduce Si surface recombination (to surface recombination velocities < 5 cm/s) on specific wafer surfaces, making them compatible with different device structures, they have their drawbacks as well. For instance, a-Si:H passivation in Si heterojunction (SHJ) cells tends to degrade at high temperature, limiting the cell processing temperature to < 300^{O}C; furthermore, it also suffers from parasitic light absorption when used as a front passivation layer [6]. SiO_2 is the most common and popular passivation material that can be grown either by dry or wet steam oxidation [7,8] at high temperatures (> 850^{O}C). However, this can deteriorate the bulk quality of the Si wafers. Plasma enhanced chemical vapor deposited (PECVD) a-SiN_X:H is more suitable for n-type Si surfaces because of its positive fixed charge density. However, for p-type surfaces, parasitic shunting is introduced due to an inversion layer [9]. In contrast, a substantial negative fixed charge density makes Al_2O_3 passivation more suitable for boron-doped (p^+) diffused surfaces [10]. Therefore, the search for alternative passivation layers has been the subject of extensive research, and detailed reviews can be found in the literature [11, 12].

In the search for an alternative passivation material comparable to the state-of-the-art oxide-based passivation, it was observed that hydrogen sulfide (H_2S) chemisorption on the Si (100) surface can passivate the dangling bonds through Si-S-Si bonding, similar to the surface chemistry of water (H_2O) with

Si [13, 14]. For H_2S gas exposure of Si(100) surfaces in an ultra-high vacuum (base pressure $\sim 4\times10^{-11}$ Torr) chamber, dissociative adsorption ($H_2S \rightarrow H+HS$) was demonstrated at temperatures ranging from -145 to 425^{O}C [15]. Using temperature-programmed desorption (TPD) and Auger electron spectroscopy (AES) measurements, desorption of hydrogen along with sulfur diffusion into the Si crystal, with formation of Si–S–Si bonds by breaking the Si dimer over the temperature range of 525 – 625^{O}C, was found [14]. Minority carrier lifetimes > 2000 μs for n-type [16] and > 250 μs for p-type Si(100) planar wafers were reported after H_2S gas phase reaction [17, 18].

In this work, the H_2S reaction passivation is applied to the n^+ diffused surface. First, the emitter saturation current density (J_0) is investigated on symmetrically n^+ diffused Si surfaces, optimally passivated by H_2S, and is compared to the passivation by state-of-the-art thermal SiO_2 and a-SiN_X:H layers. After achieving superior passivation quality with low J_0, the H_2S passivation is applied to the emitter surfaces of p-PERC cell structures, with the back surface passivated by traditional Al_2O_3. An implied (i.e., indirectly measured) V_{OC} > 680 mV is achieved in the finished PERC cell structure before applying the metal contacts, demonstrating the potential of effective S-passivation. A systematic study of changes in passivation quality after each processing step and a detailed surface analysis were carried out to gain insights into the passivation (and degradation) mechanism.

II. EXPERIMENT

To assess the surface passivation quality of phosphorous (n^+) diffused wafers, quantified by J_0, n-type industrial textured Czochralski (Cz) Si wafers with a thickness of 190 µm and a resistivity of 3 Ω-cm were used. Symmetric-dopant diffused surfaces (n^+–n–n^+) were prepared by phosphorous doping using phosphorous oxychloride ($POCl_3$) to form junctions on both sides with sheet resistances (R_{sheet}) of ~60 Ω/sq. After dopant diffusion, the wafers went through a glass removal/cleaning step in dilute hydrofluoric acid (HF) solution, and the R_{sheet} of the diffused layer was measured on clean wafers by a 4-point probe. The surface oxide was removed in 10% HF solution for 1 min before loading the wafers into the reaction chamber. The reaction chamber was then pumped down to < $1x10^{-6}$ Torr to reduce atmospheric impurities. The dopant-diffused wafer surfaces were passivated by reacting in a 3.4% H_2S – argon (Ar) gas mixture at 550^{O}C for 60 mins at atmospheric pressure (~ 760 Torr). Optimized H_2S reaction conditions and details of the thermal H_2S CVD reactor are reported elsewhere [16]. The sister wafers were passivated by state-of-the-art thermal SiO_2, grown at 855^{O}C, and by PECVD-grown a-SiN_X:H at 300^{O}C (referred to as "LTN") and 450^{O}C (referred to as "HTN") for comparison. The J_0 values were estimated by quasi-steady-state photoconductance (QSSPC), using a Sinton WCT-100 tool, from the slope of the injection level dependent inverse lifetime curves [18, 19].

To fabricate the p-PERC solar cell structures, 24 pieces of 160 µm boron-doped p-type Cz Si wafers with resistivity of 2 Ω-cm were prepared. The wafer preparation procedures are shown in Fig. 1 (steps 1-4). The wafers were then divided into two sets: a) 12 pieces for reference PERC and b) 12 pieces for sulfur-passivated emitter PERC. The primary difference in the process sequence between the two sets was that the reference PERC wafers received front n^+ emitter surface passivation by thermal SiO_2, deposited at 855^{O}C and capped with a-SiN_x:H (step 5a and 6a), while the other wafers received a rear planar surface passivation by atomic layer deposition (ALD) Al_2O_3 and a PECVD a-SiN_x:H layer stack (steps 5b and 6b). The wafers were then laser cut into 75 x 37 mm^2 pieces, and two 2 x 2 cm^2 cells were fabricated from each 75 x 37 mm^2 wafer. In order to obtain a reference point for the 2 x 2 cm^2 cells, a large-area (244.3 cm^2) cell using the same emitters and reference a-SiN_x:H passivation was fabricated. Then, sister wafers were used to fabricate the small-area (4 cm^2) cells according to the process shown in Fig. 1. The contact firing temperature of the small cells was carefully calibrated and matched to the large-area cells using thermocouple contact profile measurements.

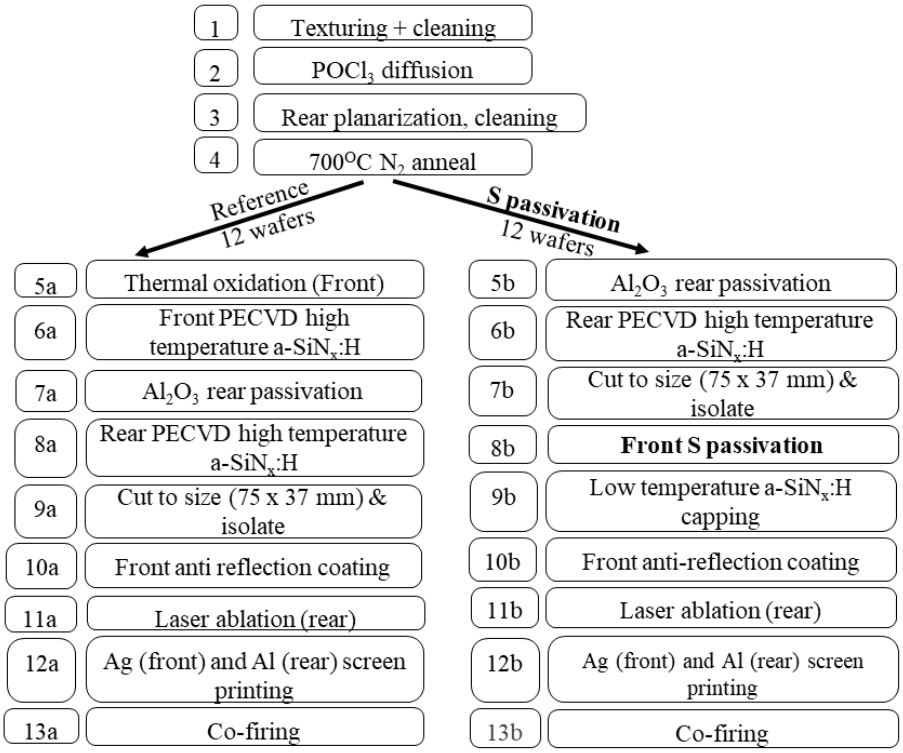

Fig. 1. Process flow of two sets of p-PERC solar cells: "reference PERC" with n^+ emitter passivated by a SiO_2/a-SiN_x:H stack (left) and "Sulfur passivated emitter PERC" with n^+ emitter passivated by H_2S gas reaction (right), as shown in step 8b (highlighted in bold font)

The 75 x 37 mm^2 size wafers were cleaned in 10% HF solution for 1 min to remove any native oxide on the exposed n^+ surface. Since only one surface (n^+ diffused emitter) of the samples needed to be passivated, sulfur passivation was performed simultaneously on two samples by loading the samples vertically back-to-back. The sulfur reaction process was the same as previously discussed above. The sulfur passivated surfaces received a 30 nm thick LTN immediately after sulfur reaction with minimal air exposure (< 5 mins), as they are thermodynamically unstable in air [16]. Three types of capping layer processes were investigated – (i) continuous deposition of LTN, referred to as "single", (ii) plasma interruption (one off/on cycle) at the halfway stage, referred to as "stack", and (iii) doubling the ammonia (NH_3) flow, referred to as "2x NH_3", keeping all other parameters constant. This was followed by HTN with a thickness of 70 nm as an antireflective coating (ARC). The rear side of the cells was then laser-patterned for local contact openings. An Ag/n^+-Si ohmic grid contact (front) and an Al/p-Si rear contact was formed by screen-printed metal paste and co-firing at a peak temperature of 760^{O}C for ~3 seconds. The finished device structure is shown in Fig. 2. Implied open-circuit voltage (iV_{OC}) values were calculated from the estimated excess carrier density (Δn) and photoconductance (σ_L) at each illumination intensity, derived by QSSPC using a Sinton WCT-100 tool [19, 20] before the rear-side laser patterning and metallization steps.

The cell V_{OC} and other performance parameters were recorded by J-V measurements under AM1.5 illumination obtained from a class AAA solar simulator.

To study the chemical surface structure after high-temperature exposure using x-ray photoelectron spectroscopy (XPS), a separate set of four n-n^+ S-passivated Si wafers was prepared. Two of the silicon wafers were capped with a 10 nm LTN, and the other two with a 30 nm LTN, using the same procedure as discussed above. Two of the silicon wafers (10 and 30 nm) were exposed to rapid thermal processing (RTP) at 700^{O}C for 2 minutes in Ar atmosphere to simulate the contact firing process. After preparation, samples were sealed in an inert atmosphere and shipped to UNLV for XPS, which was performed with a SPECS PHOIBOS 150 MCD electron analyzer and a SPECS XR 50 Mg K_α x-ray source [21]. The electron analyzer was calibrated according to [22]. Finally, the surface morphology of the sulfur-passivated Si wafers was studied before and after RTP by scanning electron microscopy (SEM) in an AMRAY 1810T SEM system.

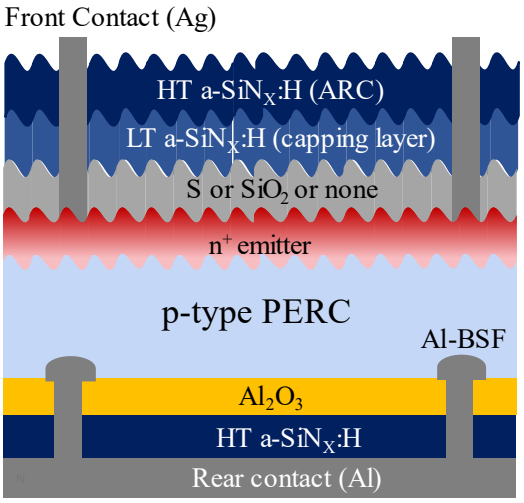

Fig. 2. Schematic of the PERC cell structure developed in this work, with the front emitter passivated by either sulfur (S), SiO_2, or none.

III. RESULTS & DISCUSSION

A. J_0 values on symmetrically n^+ diffused surfaces

The J_0 values of symmetrically diffused n^+ wafers (J_{0n+}) were estimated from the slope of the inverse effective lifetime ($1/\tau_{eff} - 1/\tau_{Auger,rad}$) as a function of excess carrier density (Δn) for Δn between 2 and 4×10^{15} cm^{-3}, as shown by the shaded region in Figure 3. The H_2S reaction shows efficient passivation of the n^+ diffused surface with J_0 = 30 fA/cm^2, which is significantly lower than the value of all other employed passivation strategies, including SiO_2+HTN. This confirms that the H_2S reaction process is very effective in passivating n^+ diffused surfaces at a relatively low temperature of 550°C, similar to surface passivation of undiffused bare Si, as reported earlier [23].

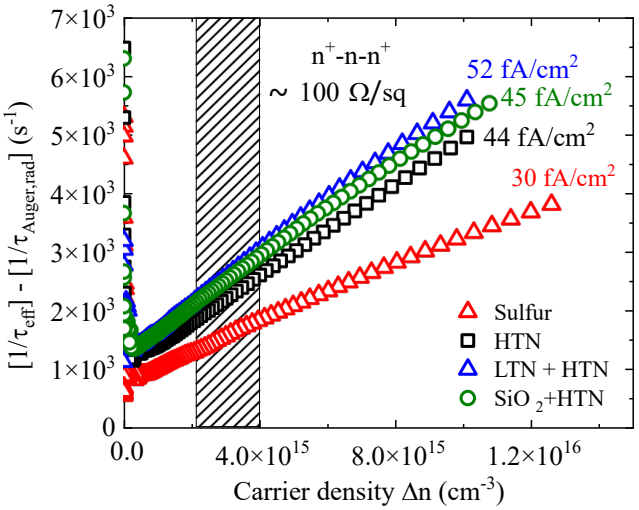

Fig. 3. Inverse effective lifetime curves as a function of excess carrier density (Δn) for symmetric n^+ diffused Si passivated by sulfur (H_2S reaction), HTN, LTN + HTN and state-of-the-art SiO_2+HTN stacks. J_0 values were estimated from the slope of the respective curves in the shaded area and are given next to each curve.

B. PERC cell fabrication with n^+ emitter passivated by H_2S reaction

After establishing good emitter surface passivation with low J_0, a series of PERC cell structures were fabricated with Al_2O_3+HTN stack passivation of the rear surface, while the top n^+ emitter surface was passivated by LTN or S + LTN. The 30 nm LTN capping layer on the S-passivated emitters was deposited with the three different processes in single, stack, and 2x NH_3 gas flow conditions. For the cell structure wafers, iV_{OC} was used as a figure of merit for the assessment of surface passivation quality, since they do not have a symmetric diffused surface. Fig. 4 shows the improvement in iV_{OC} after sulfur passivation as a function of different nitride capping layer deposition conditions. It represents iV_{OC} values of wafers without and with sulfur passivation, respectively. The figure clearly shows that the addition of S-passivation at the emitter surface improves iV_{OC} from 628 to ~680 mV, independent of the specific choice of capping layer process studied in this work.

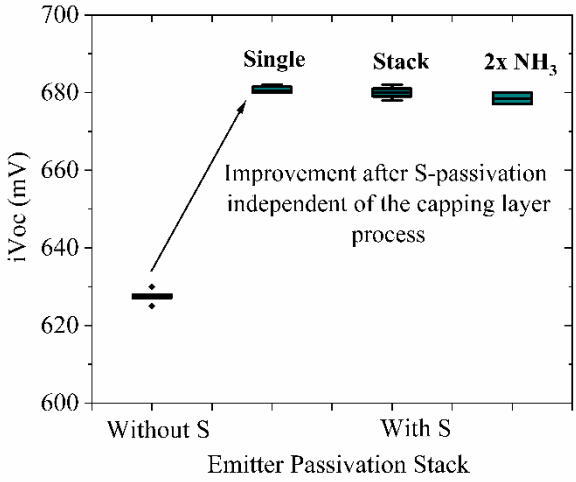

Fig. 4. iV_{OC} recorded at 1-sun intensity of PERC test cell structures without and with sulfur passivation on the emitter surface and with different capping layer processes (single, stack, and 2x NH_3, with NH_3/SiH_4 flow ratios of 4, 4, and 8, respectively). Each set of data points consist of at least five samples of size 75 x 37 mm^2.

The solar-cell devices were completed by applying different passivating processes to the front emitter and screen-printing metal contacts. First, we compare the performances of large- (244.3 cm^2) and small-area (4 cm^2) cells with HTN emitter passivation. The small-area cells were delineated by laser scribing either at the front (emitter) or rear (contact) side of the cell. Table 1 compares the cell parameters. The large-area reference PERC cell achieved a cell efficiency of 21.4%, while the small-area cells on sister wafers using the same passivation processes yielded slightly lower efficiencies, likely due to enhanced edge recombination (i.e., due to the larger edge-to-

cell area ratio in the small cells). The front isolation scribe decreases the fill factor (FF) and increases the diode ideality factor (n-factor) significantly more than the rear isolation scribe, resulting in >1.5% absolute loss in efficiency for front isolation and ~ 0.7% for rear isolation. Nevertheless, the rear isolation provides higher efficiency in small-area cells, with improved FF and lower ideality factor, than the front isolation.

TABLE I

J-V parameters of the reference large-area (244.3 cm^2) cell and best J-V parameters for small-area (4 cm^2) cells with HTN as emitter passivation. The front isolation laser scribe leads to a higher ideality factor (n-factor) and lower fill factor (FF) than the rear isolation scribe.

Cell Area	Laser Scribing	V_{OC} (mV)	J_{SC} (mA/cm^2)	Eff (%)	FF (%)	n-factor
Full area (244.3 cm^2)	Reference PERC	673	40.55	21.44	78.58	1.06
Small area (4 cm^2)	Front scribe	670	40.15	19.57	72.71	1.61
	Rear scribe	664	40.55	20.76	77.14	1.24

The minority carriers generated at the front surface suffer less recombination loss due to edge isolation damage created only at the rear surface. Therefore, a series of small cells with rear isolation scribe were fabricated with different front emitter passivation structures, i.e., HTN, SiO_2 + HTN, LTN + HTN, and S + LTN + HTN. Fig. 5 shows the grouped box charts for small-area (4 cm^2) PERC cell efficiency distributions as a function of the different emitter passivation stacks. The box charts represent cell efficiencies with sulfur-free and sulfur-containing emitter passivation, respectively. There are 10 cells in each category. An efficiency of ≥ 20% is achieved for cells with a-SiN_x:H-based (HTN and LTN + HTN) emitter passivation, while the S-passivated emitter cells had efficiencies < 20%.

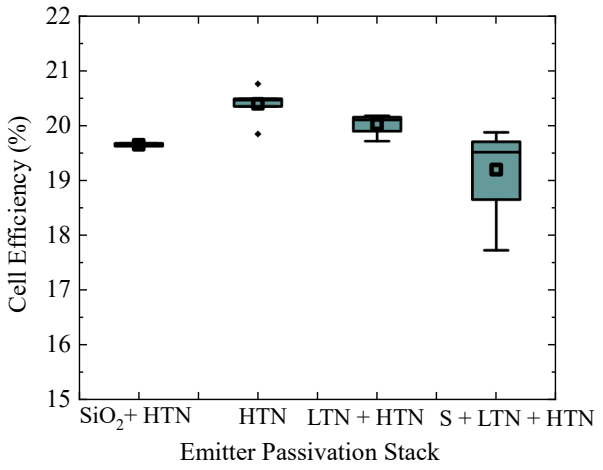

Fig. 5. Grouped box plot for PERC solar-cell efficiencies (4 cm^2) for different emitter passivation stacks.

Fig. 6 shows the current-voltage (J-V) curves for the best cells with HTN, SiO_2+HTN, and S+LTN+HTN passivation stack, respectively. The inset of Fig. 6 lists the J-V parameters of the respective cells. It is clearly seen that the slightly lower efficiency of the S-passivated emitter cell is caused primarily by lower V_{OC}. This is in contrast to the results shown in Fig. 4, where the S-passivated emitter structure exhibited superior emitter passivation with higher iV_{OC} before metallization.

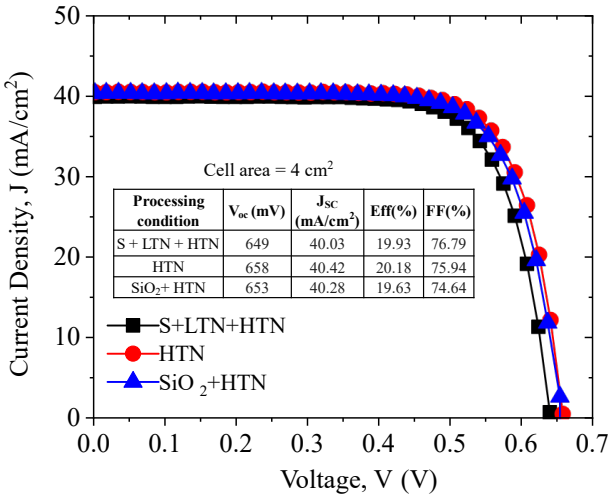

Fig. 6. Light J-V curves for completed PERC cells with emitter passivated by three different stack structures.

A direct comparison between iV_{OC} (black) and measured V_{OC} (red) on completed small-area (4 cm^2) cells is shown in Fig. 7. The cell V_{OC} increases by ≈ 25 mV from the pre-metallization iV_{OC} values for the emitter passivated by LTN+HTN. This observed improvement is presumably due to an improvement of both bulk and surface passivation caused by hydrogenation from a-SiN_x:H during the contact firing process, as described in literature [24, 25, 26]. However, the S-passivated emitter cells exhibit a drop in cell V_{OC} (> 30 mV), compared to their respective iV_{OC} values. This suggests a severe degradation of the passivation during cell fabrication for the S-passivated emitter structures.

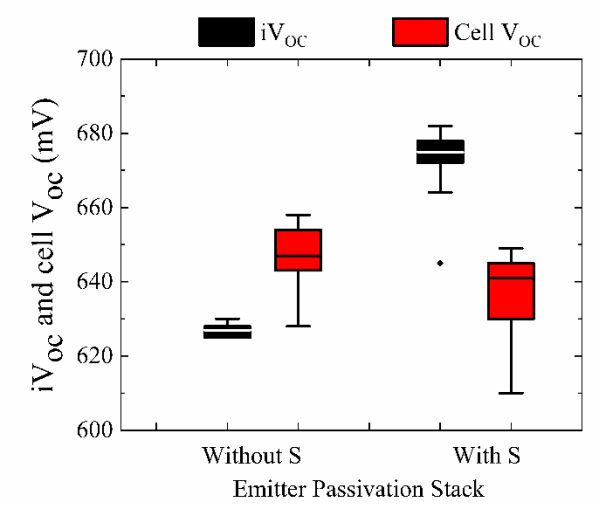

Fig. 7. iV$_{oc}$ before metallization and rear patterning (black), and measured PERC cell V$_{OC}$ of completed cells under AM1.5 illumination after metallization (red).

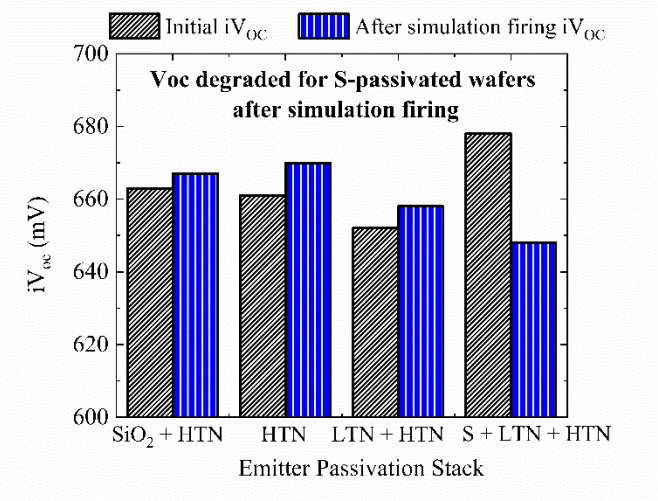

Fig. 8. Comparison of iV$_{OC}$ before (black) and after simulation firing (blue) of the PERC cell structures (without metal and rear pattern) with emitter passivated by different stacks.

C. Identifying causes of S-passivation loss

To identify the cause of the above-discussed S-passivation loss, some cell structures were exposed to RTP (fired) in the belt furnace without any metal and laser patterning on the rear side, which is referred to as "simulation firing". Fig. 8 compares the variations in iV$_{OC}$ before and after the simulation firing with front n$^+$ emitter passivated in four different structures: SiO$_2$ + HTN, HTN, LTN, and S + LTN + HTN. Structures with sulfur passivation had an initial (i.e., before simulation firing) iVoc of ~ 680 mV, demonstrating excellent n$^+$ surface passivation by sulfur. In comparison, SiO$_2$ + HTN and HTN passivated emitter surfaces yielded an iV$_{OC}$ of ~660 mV.

A severe degradation of the sulfur passivation is observed after the simulation firing process, as indicated by iVoc dropping to ~ 645 mV. This clearly indicates that the relatively low efficiency (Fig. 5) and the loss in cell V$_{OC}$ (Fig. 7) are primarily due to degradation of the sulfur passivation at the emitter surface during the contact firing step. In contrast, the emitter surface passivated by SiO$_2$ + HTN, HTN, and LTN all show slight improvements in iV$_{OC}$ after the simulation firing. This is presumably due to hydrogen diffusion from the hydrogenated a-SiN$_x$:H films to the emitter surface, thus improving surface-defect passivation [26].

To further investigate such degradation of S-passivated cells during simulation firing, XPS was performed on S-passivated n-n$^+$ silicon surfaces with an LTN capping layer (10 and 30 nm). Figure 9 shows the survey spectra of these silicon wafers, with and without RTP. All expected peaks are present, such as nitrogen-, silicon-, and weak sulfur-related signals. A significant amount of oxygen is observed on the surface without RTP. After RTP, the oxygen signal further increases for both "10 nm" and "30 nm" samples. Gallium and sodium are also found after RTP of the "10 nm" sample, likely due to residues in the RTP chamber. Zinc is a common trace metal in silicon and the presence of fluorine can be attributed to the use of HF during the cleaning process.

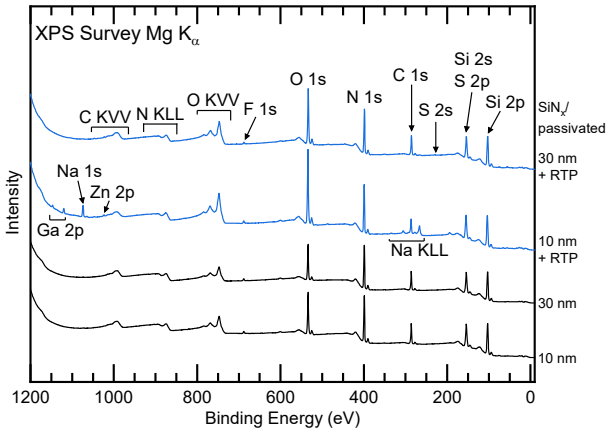

Fig. 9. Mg K$_\alpha$ XPS survey spectra of the sulfur-passivated n-n$^+$ silicon surfaces with a 10 and 30 nm LTN capping layer, before and after RTP. Prominent photoemission and Auger peaks are labeled.

Figure 10 shows the S 2s XPS detail region. For the samples without RTP, a weak sulfur signal is visible in both the "10 nm" and "30 nm" samples. In comparison with established reference systems [22] (as indicated by the gray bars in Fig. 10), the sulfur

is found to be bonded in an S-O bonding environment. This is corroborated by the significant presence of oxygen on the sample surface. After RTP, an increase in the sulfur intensity is visible in both samples, and the spectral weight shifts to higher binding energies, i.e., to a more oxidized environment. These observations suggest a diffusion of sulfur towards the SiN_x surface and/or modification of the SiN_x layer (e.g., thinning, formation of islands or pinholes) due to the high temperature exposure during RTP, coupled with the additional incorporation of oxygen from the RTP environment.

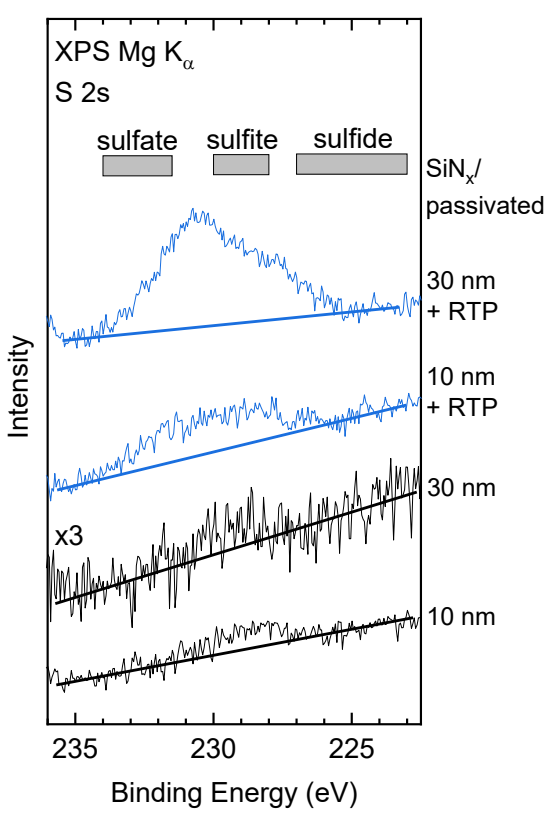

Fig. 10. XPS detail region of the S 2s core level. Gray bars represent typical binding energies for various chemical environments of sulfur [22]. A linear background is drawn for each of the spectra to help identify the presence of sulfur. The spectrum of the "30 nm" sample was multiplied by a factor of 3.

Finally, Figure 11 (a) and (b) compare the SEM images of a sample passivated by S + LTN (30 nm) before and after RTP. Fig. 11 (a) shows a flat and featureless surface, with only one (presumably dust) particle being visible. In contrast, the same sample after RTP shows many distinct bright circular spots of diameter 0.5-1 µm, which is attributed to pinholes in the LTN film, corroborating the interpretation of the XPS results that pinholes might contribute to the increased sulfur concentration at the sample surface after RTP.

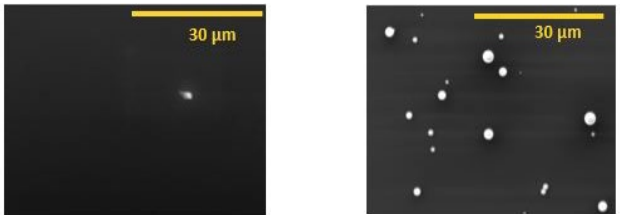

(a) Before RTP (b) After RTP

Fig. 11. Scanning electron microscopy images of 30 nm LTN (a) before, and (b) after RTP at 760^{O}C for ~5 seconds. The white spots on the sample surface after RTP can be identified as pinholes of diameter 0.5-1 µm.

IV. CONCLUSION

In this work, chemical passivation of sulfur was applied to small-area (4 cm^2) passivated emitter and rear contact (PERC) cells. A J_0 = 30 fA/cm^2 was achieved by sulfur passivation using H_2S reaction on symmetrically n^+ diffused emitters ($R_{sheet,n+}$ ~ 100 Ω/sq). An implied V_{OC} ≈ 680 mV (highest 686 mV) was demonstrated with the application of S-passivation to the emitter surface in the PERC cell structure (with the rear surface passivated by an aluminum oxide (Al_2O_3)/a-SiN_x:H stack). The S-passivation was found to be better than the a-SiN_x:H or SiO_2/a-SiN_x:H passivated emitter surface. However, a substantial drop in the cell V_{OC} was observed for the S-passivated PERC cell after the completion of device fabrication with laser patterning, screen-printed metal contact deposition, and RTP firing. An efficiency ≈ 20% and V_{OC} ≈ 650 mV was achieved with an emitter surface passivated by sulfur. Detailed surface analysis using XPS suggests the diffusion of sulfur and/or modification of the SiN_x layer after high-temperature exposure in the contact firing process, the latter being corroborated by SEM results.

ACKNOWLEDGEMENT

The authors are thankful to William N. Shafarman for his assistance in designing experiments and his overall support throughout the entire work. This work was supported by the US Department of Energy's Office of Energy Efficiency and Renewable Energy (EERE) under the Solar Energy Technologies Office (SETO) Agreement Number DE-EE0008554.

expressed herein do not necessarily state or reflect those of the United States Government or any agency thereof."

REFERENCES

[1] T. Dullweber and J. Schmidt, "Industrial Silicon Solar Cells Applying the Passivated Emitter and Rear Cell (PERC) Concept—A Review," in *IEEE Journal of Photovoltaics* **6**, 5, 1366-1381, 2016, doi: 10.1109/JPHOTOV.2016.2571627.

[2] A. Blakers, "Development of the PERC Solar Cell," in *IEEE Journal of Photovoltaics* **9**, 3, 629-635, 2019, doi: 10.1109/JPHOTOV.2019.2899460.

[3] https://www.pv-magazine.com/2022/07/13/trina-solar-achieves-24-5-efficiency-for-210-mm-p-type-perc-solar-cell/(last access date: 07/05/2023)

[4] R. S. Bonilla, B. Hoex, P. Hamer, P. R. Wilshaw, "Dielectric surface passivation for silicon solar cells: A review"*, Phys. Status Solidi A* **214**, 1700293, 2017, doi: 10.1002/pssa.201700293

[5] V. I. Kuznetsov, M. A. Ernst and E. H. A. Granneman, "Al_2O_3 surface passivation of silicon solar cells by low-cost ALD technology," *2014 IEEE 40th Photovoltaic Specialist Conference (PVSC)*, Denver, CO, USA, 0608-0611, 2014, doi: 10.1109/PVSC.2014.6924995.

[6] Z. C. Holman, A. Descoeudres, L. Barraud, F. Z. Fernandez, J. P. Seif, S. D. Wolf, and C. Ballif, "Current Losses at the Front of Silicon Heterojunction Solar Cells", in *IEEE Journal of Photovoltaics* **2**, 1, 7-15, 2012, doi: 10.1109/JPHOTOV.2011.2174967.

[7] A. G. Aberle, S. W. Glunz, A. W. Stephens, and M. A. Green, "High-efficiency Si Solar Cell: Si/SiO_2 interface parameters and their impact on device performance," *Prog. Photovolt: Res. Appl.* **2**, 265, 1994, doi: 10.1002/pip.4670020402.

[8] J. Benick, K. Zimmermann, J. Spiegelman, M. Hermle and S W Glunz, "Rear side passivation of PERC-type solar cells by wet oxides grown from purified steam," *Prog. Photovolt: Res. Appl.* **19**, 361, 2011, doi: 10.1002/pip.1020.

[9] J. R. Elmiger and M. Kunst, "Investigation of charge carrier injection in silicon nitride/silicon junctions," *Appl. Phys. Lett.* **69**, 4, 517–519, 1996, doi:10.1063/1.117772

[10] J. Schmidt, A. Merkle, R. Brendel, B. Hoex, M. C. M. van de Sanden; W. M. M. Kessels, "Surface passivation of high-efficiency silicon solar cells by atomic-layer-deposited Al_2O_3" *Prog. Photovolt: Res. Appl.* **16**, 6, 461–466, 2008, doi:10.1002/pip.823.

[11] L. E. Black, B. W. H. van de Loo, B. Macco, J. Melskens, W. J. H. Berghuis, and W. M. M. Kessels, "Explorative studies of novel silicon surface passivation materials: Considerations and lessons learned," *Solar Energy Materials and Solar Cells* **188**, 182, 2018, doi:10.1016/j.solmat.2018.07.003.

[12] J. Schmidt, R. Peibst, R. Brendel, "Surface passivation of crystalline silicon solar cells: Present and future", *Solar Energy Materials and Solar Cells* **187**, 39–54, 2018, doi:10.1016/j.solmat.2018.06.047.

[13] V. Barone, "The cluster approach in the study of atomic and molecular chemisorption on silicon", *Surface Science* **189-190**, 106–113, 1987, doi:10.1016/s0039-6028(87)80420-x.

[14] M. Tao, D. Udeshi, N. Basit, E. Maldonado, and W. P. Kirk, "Low Schottky barriers on n-type silicon (001)", *Appl. Phys. Lett.* **83**, 2593, 2003, doi:10.1063/1.1613357.

[15] M. Han, Y. Luo, N. Camillone, and R. M. Osgood, "Reaction of H_2S with Si (100)", *J. Phys. Chem* B **104**, 6576, 2000, doi:10.1021/jp0002446.

[16] H-Y. Liu, U. K. Das, and R. W. Birkmire, "Surface Defect Passivation and reaction of c-Si in H_2S", *Langmuir* **33**, 14580, 2017, doi:10.1021/acs.langmuir.7b03520.

[17] U. K. Das, R. Theisen, G. Hanket, A. Upadhyaya, A. Rohatgi, A. Hua, L. Weinhardt, D. Hauschild, and C. Heske, "Sulfurization as a promising surface passivation approach for both n-and p-type Si", *47th IEEE PVSC Conf. Proc.* p 1167, 2020, doi: 10.1109/PVSC45281.2020.9300395.

[18] U. K. Das, R. Theisen, A. Hua, A. Upadhyaya, I. Lam, T. K. Mouri, N. Jiang, D. Hauschild, L. Weinhardt, W. Yang, A. Rohatgi, and C. Heske, "Efficient passivation of n-type and p-type silicon surface defects by hydrogen sulfide gas reaction", *J. Phys.: Condens. Matter* **33**, 464002, 2021, doi: 10.1088/1361-648X/ac1ec8.

[19] R. A. Sinton and A. Cuevas, "Contactless determination of current–voltage characteristics and minority-carrier lifetimes in semiconductors from quasi-steady-state photoconductance data", *Appl. Phys. Lett.* **69**, 2510, 1996, doi: 10.1063/1.117723

[20] A. Cuevas and D. Macdonald, "Measuring and interpreting the lifetime of silicon wafers", *Sol. Energy* **76**, 255, 2004, doi:10.1016/j.solener.2003.07.033.

[21] L. Weinhardt, D. Hauschild, and C. Heske, "Surface and interface properties in thin-film solar cells: using soft x-rays and electrons to unravel the electronic and chemical structure", *Advanced Materials* **31**, 1806660, 2019, doi:10.1002/adma.201806660.

[22] J.F. Moulder, W.F. Stickle, P.E. Sobol, and K.D. Bomben, "Handbook of x-ray photoelectron spectroscopy," Physical Electronics Division, Perkin-Elmer:Eden Prairie, MN, USA, pp. 15, 1992.

[23] U. K. Das, T. K. Mouri, R. Theisen, Y. W. Ok, A. Upadhyaya and A. Rohatgi, "Dopant diffused Si surface passivation by H_2S gas reaction and quinhydrone-methanol treatment," *2021 IEEE 48th Photovoltaic Specialists Conference (PVSC)*, pp. 1355-1358, 2021, doi: 10.1109/PVSC43889.2021.9518880

[24] Z. Hameiri, L. Mai, N. Borojevic, S. Javid, B. Tjahjono, S. Wang, A. Sproul, S. Wenham, "The influence of silicon nitride layer parameters on the implied V_{oc} of Cz silicon wafers after annealing", *34th IEEE Photovoltaic Specialists Conference (PVSC)*, pp. 001795-001800, 2009, doi: 10.1109/PVSC.2009.5411485

[25] A. Ebong, P. Doshi, S. Narasimha, A. Rohatgi, J. Wang, and M. A. El-Sayed, "The effect of low and high temperature anneals on the hydrogen content and passivation of Si surface coated with SiO_2 and SiN films", Journal of The Electrochemical Society **146**, 5, 1921-1924, 1999, doi: 10.1149/1.1391866

[26] A. M. O. M. Okasha, B. Kafle, B. Torda, C. Teßmann, and M. Hofmann, "Optimized amorphous silicon nitride layers for the front side passivation of c-Si PERC solar cells", EPJ Photovoltaics **11**, 6 2020, doi:10.1051/epjpv/2020003